

Anomalous adsorption of biomolecules on a Zn-based metal-organic framework obtained via a facile room-temperature route

Alexandr V. Vinogradov^{*a}, Haldor Zaake-Hertling^b, Andrey S. Drozdov^a, Peter Lönnecke^b, Gulaim A. Seisenbaeva^c, Vadim G. Kessler^c, Vladimir V. Vinogradov^a and Evamarie Hey-Hawkins^{*b}

^a ITMO University, St.Petersburg, Russia

^b Leipzig University, Leipzig, Germany

^c Swedish University of Agricultural Sciences, Uppsala, Sweden

1. A new method for crystal growth based on slow diffusion conditions created by a flow gradient in liquids separated with a gas layer

1.1. Formation of the product

A study on the peculiarities of crystallization employing this method was carried out using crystallization of metal-organic frameworks as an example (Fig. 2). For this purpose, solutions of ligands and metal precursors were prepared in separate beakers. Given the dynamic mobility of ions of a ligand (depending on the structure), its solution with a preset concentration was placed inside vessel 2, and the metal precursor solution was poured from the beaker into vessel 3 directly after connecting vessel 2 with it. Heating the glass sphere was carried out in the range from 80 to 120 °C (depending on the viscosity of the solutions). It should be taken into account that the temperature variation determines not only the magnitude of the negative pressure in vessel 2 after cooling the sphere, but also the equilibration time for the system (Fig. S1) due to the long cooling of rarefied gas because of the low heat transfer through the capillary (Fig. 2).

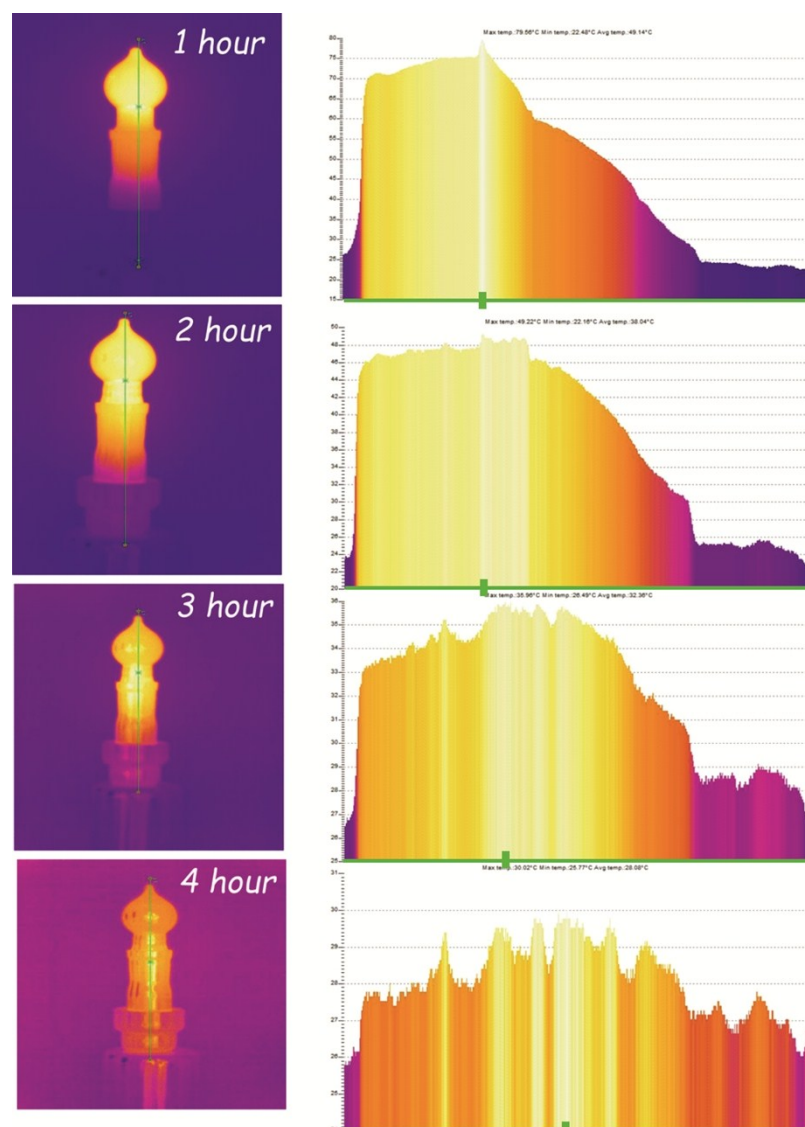


Figure S1. Left-side: Device temperature gradient vs. time. Right-side: temperature distribution vs. green line.

Experimental results obtained using solutions of terephthalic acid and zinc acetate, as well as zinc acetate and a pyrene-based ligand ($H_4TBAPy = 1,3,6,8$ -tetrakis(*p*-benzoic acid)pyrene), are shown in Figures S2 and S3, respectively. The formation of single crystals suitable for various methods of physicochemical analysis can be clearly observed.

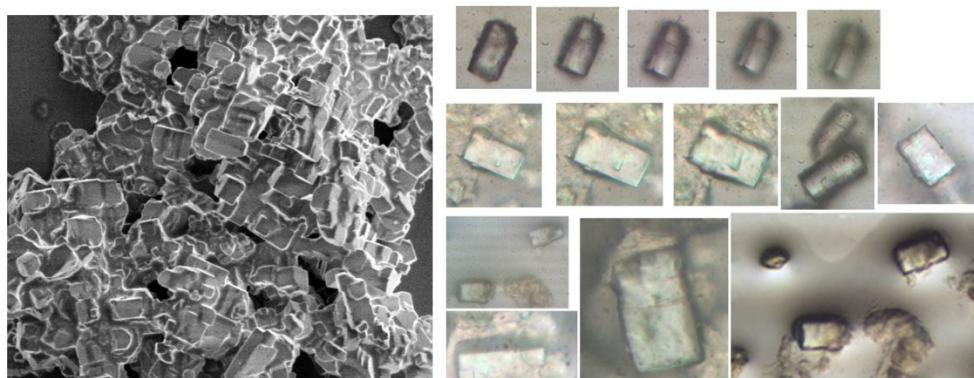


Figure S2. Optical and SEM images of crystals of MOF-5⁴ which were obtained using the described method.

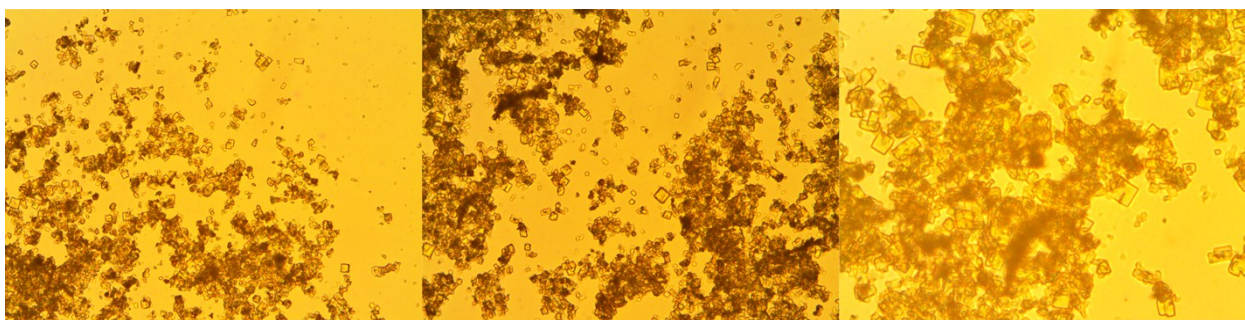


Figure S3. Optical and SEM images of crystals of $[\{Zn_2(TBAPy)(H_2O)_2\} \cdot 3.5DEF]_n$ (**1**) which were obtained using the described method.

The method described here is based on new principles that provide slow diffusion conditions through the formation of a flow gradient in fluids separated by a gas layer. This method is applicable for the crystallization of various species and does not require high temperatures and pressures. Lack of membrane layers facilitates a simple isolation of the final product without mechanical damage. The formation of single crystals is controlled in the preparatory phase and directly during the experiment.

2. Experimental conditions

*Synthesis of $[\{Zn_2(TBAPy)(H_2O)_2\} \cdot 3.5DEF]_n$ (**1**)*

Sources of Chemicals

All experiments referred to in this work were carried out using washed and dried crystals of MOF-5 and **1**. The description of methods for their production is given in the ESI. The obtained crystals were characterized extensively with transmission electron microscopy (TEM), X-ray diffraction (XRD), and low-temperature nitrogen adsorption-desorption measurements. L-Histidine (Sigma-Aldrich 99.5% certified ACS plus) solutions were prepared using bidistilled water ($R = 18 \text{ M}\Omega$).

A new room-temperature technique for crystal growth of MOFs

Crystals of MOF-5 and $[\{Zn_2(TBAPy)(H_2O)_2\} \cdot 3.5DEF]_n$ (**1**) (TBAPy = 1,3,6,8-tetrakis(*p*-benzoate)pyrene) were obtained using a new method based on slow diffusion conditions created by the flow gradient in liquids separated by a gas layer (represented in ESI). Solvent removal was carried out in a vacuum degasser for MOF-5 at 100 °C and for **1** at 220 °C during of 24 hours, forming the respective solvent-free crystals $[Zn_4O(O_2C-C_6H_4-CO_2)_3]_n$ (**2**) and $[Zn_2(TBAPy)]_n$ (**3**), respectively.

Preparation of biocomposites His@MOF was carried out by adsorption of the L-histidine from aqueous media. It is well known that zinc(II) forms strong complexes with L-histidine in common biological systems. Complexation constants and energy (ΔG) of zinc(II)-histidine significantly exceeds the zinc(II)-aqua complex. To this end, dried crystals of MOF-5 and **1** (5 g/L) (compounds **2** and **3**) were added to an L-histidine solution (0.5 mM) in H_2O and mixed for 20 min to achieve the adsorption equilibrium.

3. Spectroscopic Studies

Attenuated Total Reflectance (ATR) FT-IR spectroscopy

Adsorption of L-histidine on dried crystals of **2** and **3** was investigated using ATR-FTIR spectroscopy. A suspension of ground crystals of **2** and **3** (1 mL of a 1.5 mg/mL solution) was directly deposited on the horizontal AMTIR (amorphous material transmitting IR radiation) crystal and dried overnight. The IR spectra of **2** and **3** before and after adsorption of L-histidine are shown in Fig. S4. It is well known that the nitrogen atoms in the imidazole group of histidine participate in coordination to a metal ion. This reaction is best detected in the range 1100–900 cm^{-1} . Fig. S7B shows the spectra of **2** and **3** after adsorption of L-histidine in detail.

In pure histidine, the in-plane vibration of the imidazole group is observed at about 964 cm^{-1} ; NH_3^+ twisting and rocking and COO^- wagging frequencies were observed in the range of 1200–600 cm^{-1} . After adsorption of L-histidine in **2** and **3**, no shift was observed in the asymmetric and symmetric stretching vibration of the carboxylate group, supporting its non-involvement in Zn coordination; however, the spectra showed a shift of the imidazole in-plane vibration to 1050 cm^{-1} , indicating coordination of imidazole to the Zn^{2+} ions, Fig. S4A, Fig. 1. A decrease in intensity of the stretching vibrations in His@**2** in contrast to those observed for His@**3** at 1050 cm^{-1} probably indicates adsorption of histidine on the surface of **2**, while for the new Zn-based MOF **3**, bulk adsorption is more likely. These conclusions are confirmed in the section for quantitative assessing sorption of L-histidine on crystals of **2** and **3**.

$[\{\text{Zn}_2(\text{TBAPy})(\text{H}_2\text{O})_2\} \cdot 3.5\text{DEF}]_n$ (**1**) was obtained by the new method described above employing two separate solutions. The solution containing 1,3,6,8-tetrakis(p-benzoic acid)pyrene (H_4TBAPy) (0.07 g, 0.1 mmol) in a mixture of DEF and ethanol (1.5 mL, 5:1) was poured inside vessel 2 (Fig. S1). The second solution containing $\text{Zn}(\text{CH}_3\text{COO})_2 \cdot 2\text{H}_2\text{O}$ (0.12 g, 0.5 mmol) in DEF (2 mL) was placed inside vessel 3 (Fig. S1). Vessel 1, which is responsible for the gradient of supplying solution 1 with solution 2, was heated to 170 $^\circ\text{C}$. The diameter of the connecting capillary was 0.7 mm at the start and 0.08 mm at its end. Two weeks later, bright yellow crystals had formed which were isolated and structurally characterized.

The IR measurements were performed using a Bruker Vertex 80v FTIR spectrometer at a resolution of 0.01 cm^{-1} . An ATR cell equipped with a ZnSe crystal (45 $^\circ$ angle of incidence) was used as the internal reflection element.

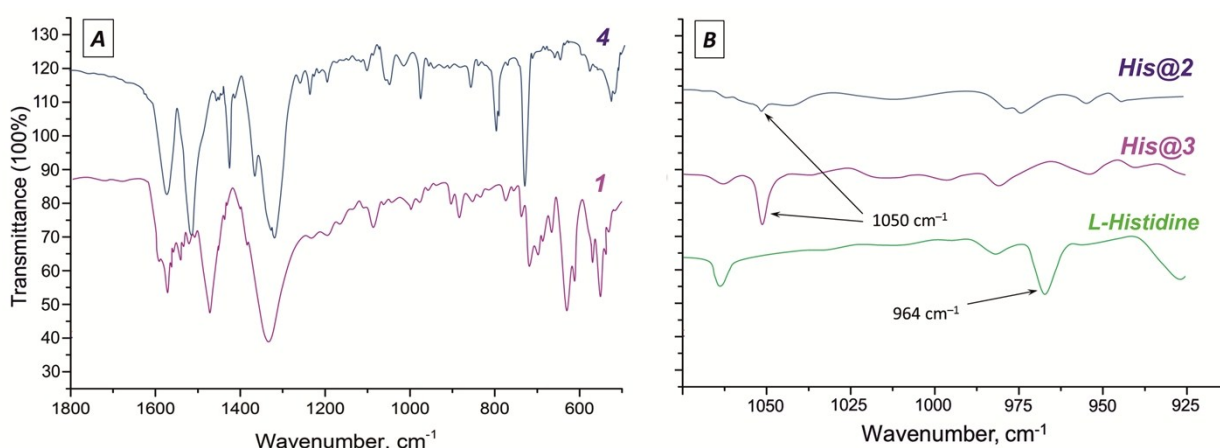


Figure S4. IR spectra: A) pure MOF-5 (**4**) and $[\{\text{Zn}_2(\text{TBAPy})(\text{H}_2\text{O})_2\} \cdot 3.5\text{DEF}]_n$ (**1**), B) dried MOF-5 (**2**) and $[\text{Zn}_2(\text{TBAPy})]_n$ (**3**) with adsorbed L-histidine.

UV-Vis spectroscopy for analyzing the concentration of adsorbed L-histidine in dried MOF-5 (2) and [Zn₂(TBAPy)]_n (3)

An analysis of adsorption curves was performed in a quartz thermostatic cuvette based on an Agilent 8454 matrix photodiode spectrophotometer. The cuvette was thermostated with a Peltier element in the range 20–50 °C.

Quantitative studies of L-histidine adsorption on crystals of **2** and **3** were conducted by UV-Vis spectroscopic investigations at 25 °C. A change in the concentration of L-histidine was estimated by a change in optical density at 280 nm upon recording kinetic spectra using a matrix photodiode detector in the range of 200–800 nm, thus providing an unequivocal identification of L-histidine adsorption from the solution. To this end, crystals of **2** and **3** (5 g/L) were added to an L-histidine solution (0.5 mM) and mixed for 20 min to achieve the adsorption equilibrium. Then, L-histidine adsorption kinetics were studied for 2 days, i.e. prior to reaching saturation. The amount of adsorbed L-histidine was calculated by determining the difference between the initial and final solution concentrations.

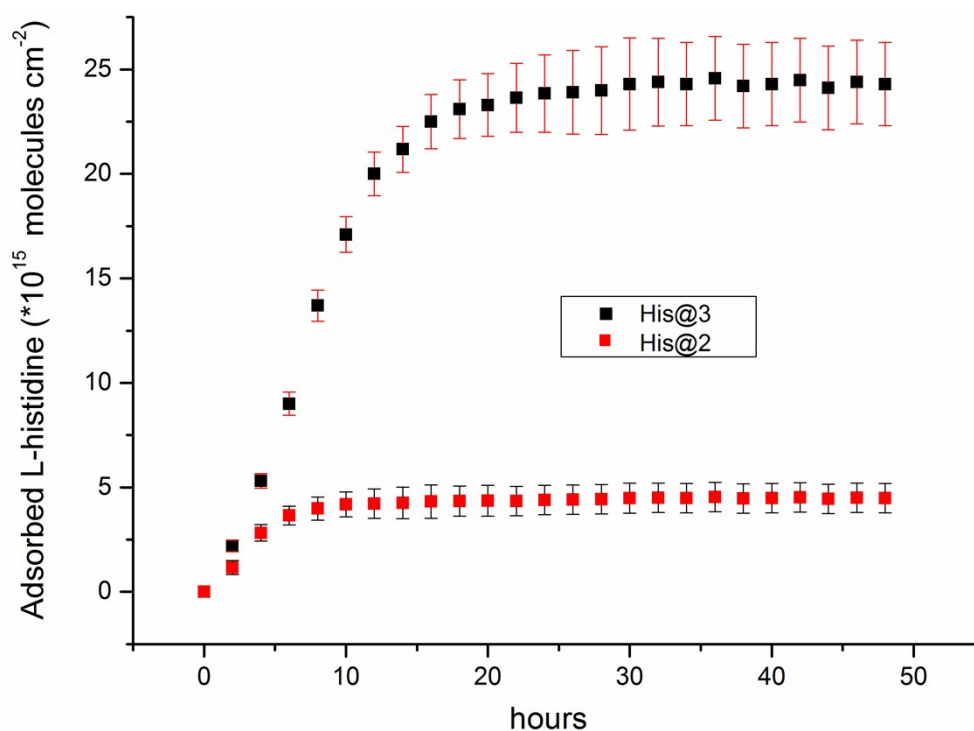


Figure S5. Adsorption isotherm for L-histidine in crystals of **2** and **3** at pH = 7.4 and T = 298 K.

Fluorescence spectroscopy

Synchronous fluorescence spectra were recorded using an Agilent Cary Eclipse spectrophotometer.

X-ray powder diffraction

To perform powder diffraction, $[\{Zn_2(TBAPy)(H_2O)_2\} \cdot 3.5DEF]_n$ (**1**) was heated at 240 °C for extracting the solvent molecules. A comparison of the powder diffraction of the prepared sample with simulated data is shown in Fig. S6, S7. Analysis of the structural data was performed with the program package Platon using $\lambda_{Cu} = 1.542 \text{ \AA}$. X-ray powder patterns were obtained using a Bruker SMART Apex-II diffractometer operating with $CuK\alpha$ radiation ($\lambda = 1.542 \text{ \AA}$).

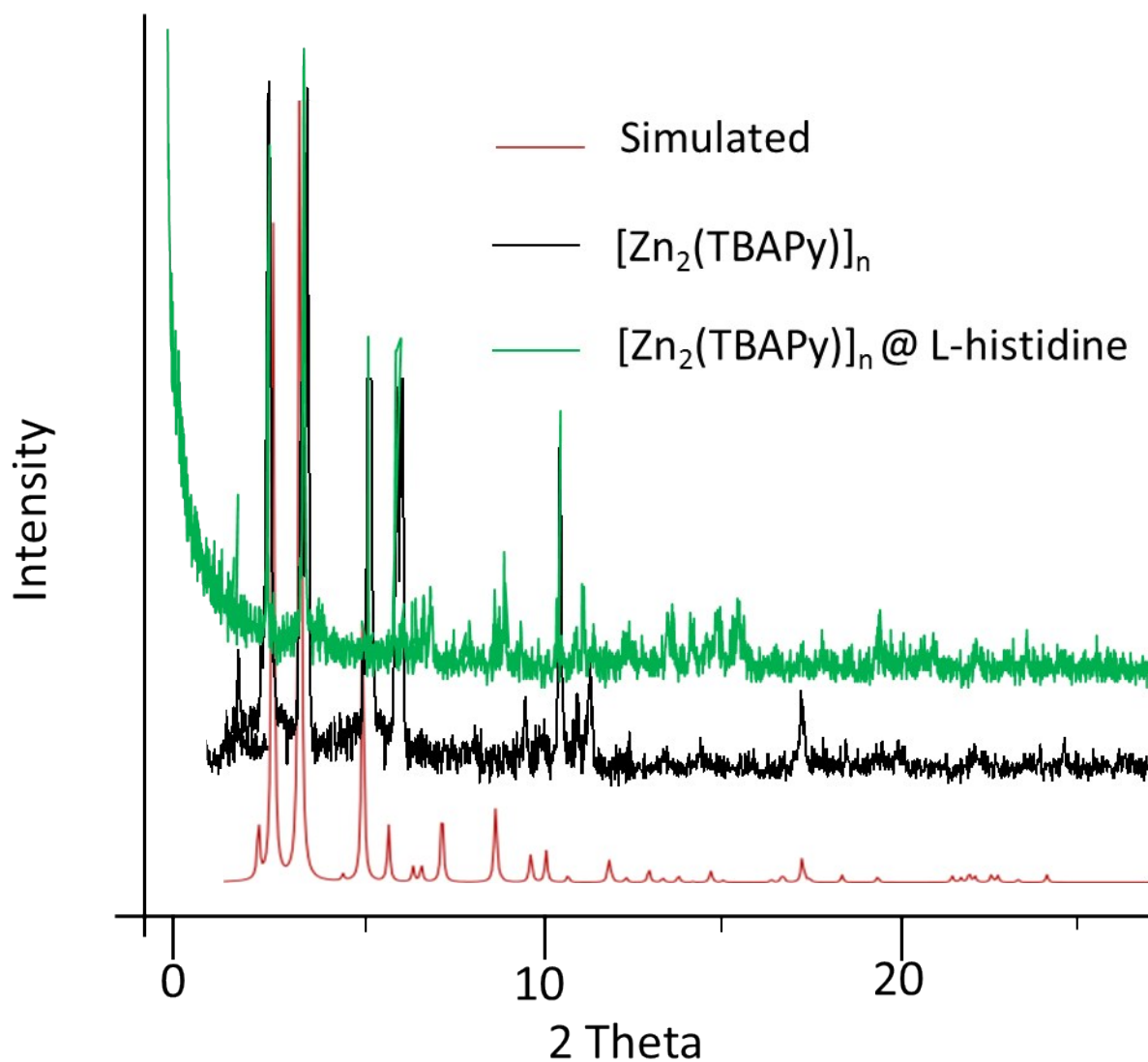


Figure S6. PXRD patterns of $[Zn_2(TBAPy)]_n$ (black), $[Zn_2(TBAPy)]_n @L\text{-histidine}$ (green line) and the simulated pattern (red).

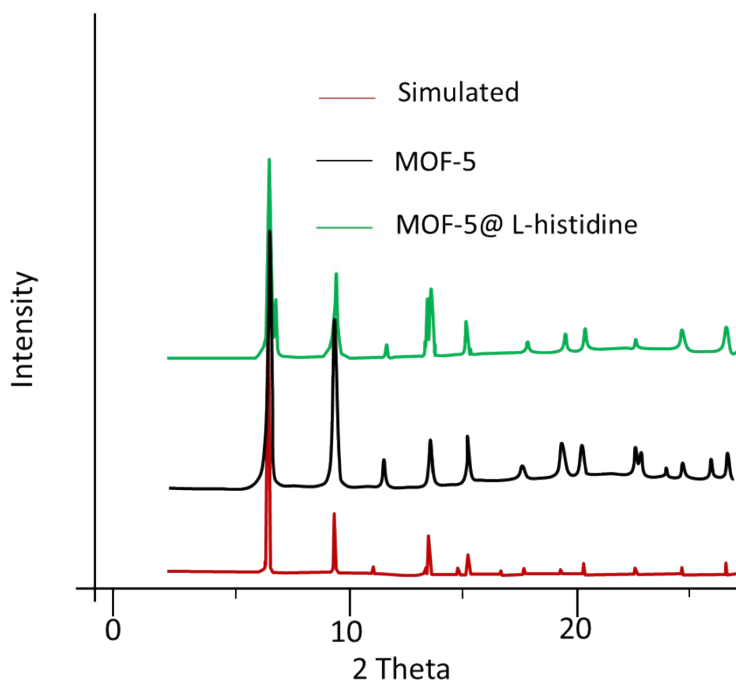


Figure S7. PXRD patterns of MOF-5, MOF-5@L-histidine (green line) and the simulated pattern (red).

Thermal analysis

Thermogravimetry analysis (TG) was carried out with $[\{Zn_2(TBAPy)(H_2O)_2\} \cdot 3.5DEF]_n$ (**1**) using an STA 449 F1 Jupiter system (Netzsch) in argon gas (at a heating rate of 3 K per minute). The mass of the sample was 10 mg.

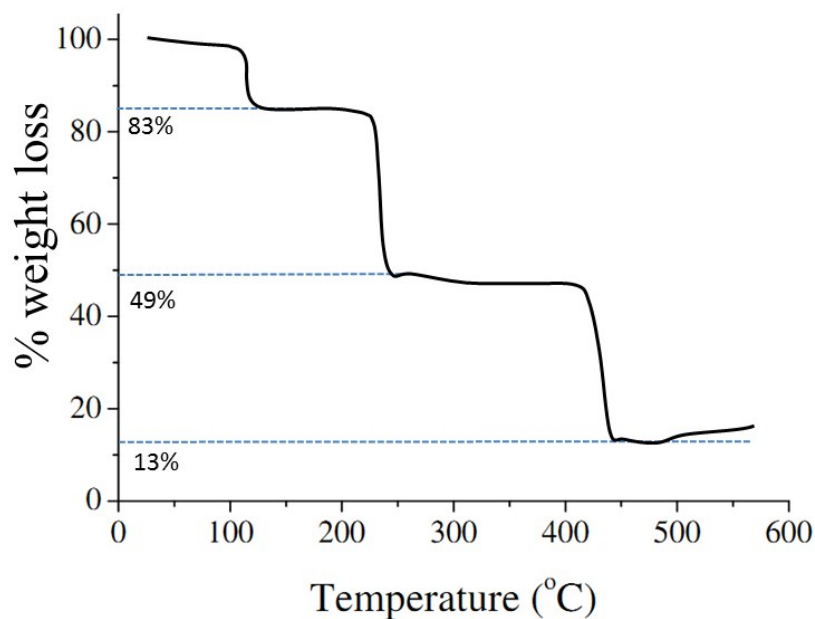


Figure S8. TG analysis of $[\{Zn_2(TBAPy)(H_2O)_2\} \cdot 3.5DEF]_n$ (**1**).

TGA showed that the removal of guest and coordinated molecules occurs in two steps with a total mass loss of 51 %. There are two clearly steps identified. The first one at 125 °C

corresponds to water and adsorbed molecules (17%). The second one at 230 °C corresponds, probably, to DEF elimination (34%). After the removal of these molecules, the framework is stable up to 415 °C. The full weight loss is 87%. Framework decomposition starts above 415 °C and occurs in a single step. The final product corresponds to ZnO.

Surface Area (Quantachrome Nova 1200)

$[\{\text{Zn}_2(\text{TBAPy})(\text{H}_2\text{O})_2\} \cdot 3.5\text{DEF}]_n$ (**1**) (20 mg) was heated under vacuum (10^{-3} torr) for 15 hours at 220 °C, fig.S9. MOF-5 and **3** before and after L-histidine adsorption was heated under vacuum (10^{-3} torr) for 15 hours at 120 °C. The specific surface area and pore size distribution have been measured using low-temperature nitrogen adsorption-desorption. The data obtained correspond to a microporous state, as confirmed by a characteristic isotherm shape (type I).¹

Although N_2 at 77 K is considered standard adsorbate when surface area and pore size are analyzed, it is nevertheless universally recognized that nitrogen adsorption is unable to give satisfactory results for quantitative assessment of porosity, especially in the ultramicropore region with a width of less than 0.7 nm.

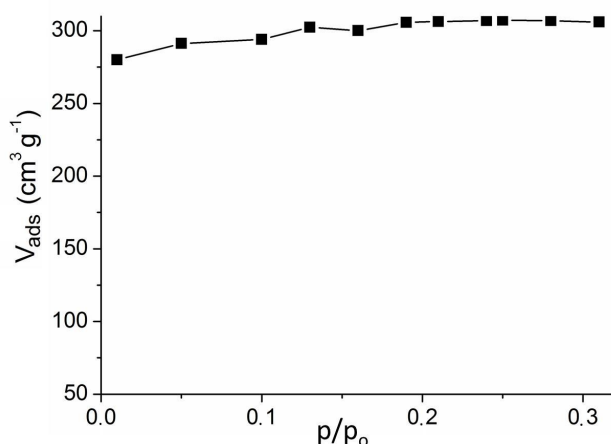


Figure S9. Nitrogen sorption isotherm of $[\text{Zn}_2(\text{TBAPy})]_n$ at $T = -196$ °C ($p_0 = 1$ atm).

The BET and Langmuir surface areas are 615 and 784 m^2g^{-1} , respectively, which are calculated using the adsorption data in the relative pressure range $p/p_0 = 0.06-0.3$. The total pore volume of $[\text{Zn}_2(\text{TBAPy})]_n$ is 0.245 cm^3/g ; pore radius $DA^2 = 0.69$ nm.

The data obtained are in accord with the values of pore volume calculated using the Platon program package. Thus, this value amounts to 0.263 cm^3 at 298 K and 0.258 cm^3 at 130 K.

Table S1. Porouse structure characterization data.

| Sample | S_{BET} , m^2g^{-1} | S_{Langmuir} , m^2g^{-1} | DA pore radius, nm |
|--|--|---|--------------------|
| $[\text{Zn}_2(\text{TBAPy})]_n$ | 615 | 784 | 0.69 |
| $[\text{Zn}_2(\text{TBAPy})]_n@L$ -histidine | 504 | 636 | 0.53 |
| MOF-5 | 1644 | 2518 | 0,43 |
| MOF-5@ L-histidine | 1118 | 1877 | 0,38 |

Dynamic Light Scattering (DLS) Aggregation Measurements

The measurements were carried out using a PhotoCor Compact-Z device. To this end, a dispersion of the materials under study was prepared. The stock solution of **2** and **3** (1 g/L) was sonicated (40% amplitude, 30 sec) to form uniform suspensions, and aliquots (30 μ L) of L-histidine were added to the histidine solutions.

A DLS analyzer was used to rule out the effect of ionic interactions between crystals of **2** or **3** and L-histidine, and also to study the processes of L-histidine aggregation on the surface of dried MOFs. The hydrodynamic diameter and zeta potential of **2** and **3** (0.05 g/L) before and after L-histidine (0.5 mM) adsorption were studied. The possibility of electrostatic interactions was assessed by a comparative analysis of the zeta potential for aqueous dispersions of **2** and **3** and L-histidine in kinetics mode during 50 hours, Fig. S12 (ESI). The stock solution of **2** and **3** (1 g/L) was sonicated (40% amplitude, 30 sec) to form uniform suspensions, and aliquots (30 μ L) of L-histidine were added to the histidine solutions

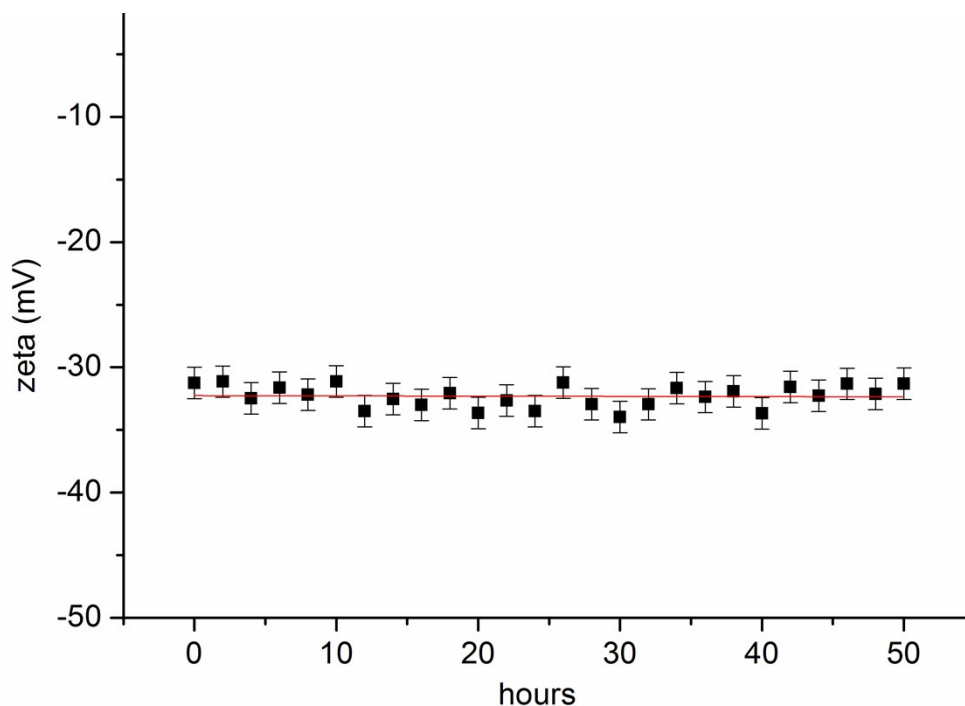


Figure S9. Change in zeta potential for L-histidine@[Zn₂(TBAPy)]_n during 50 hours at 25 °C.

2.7 Pore parameters

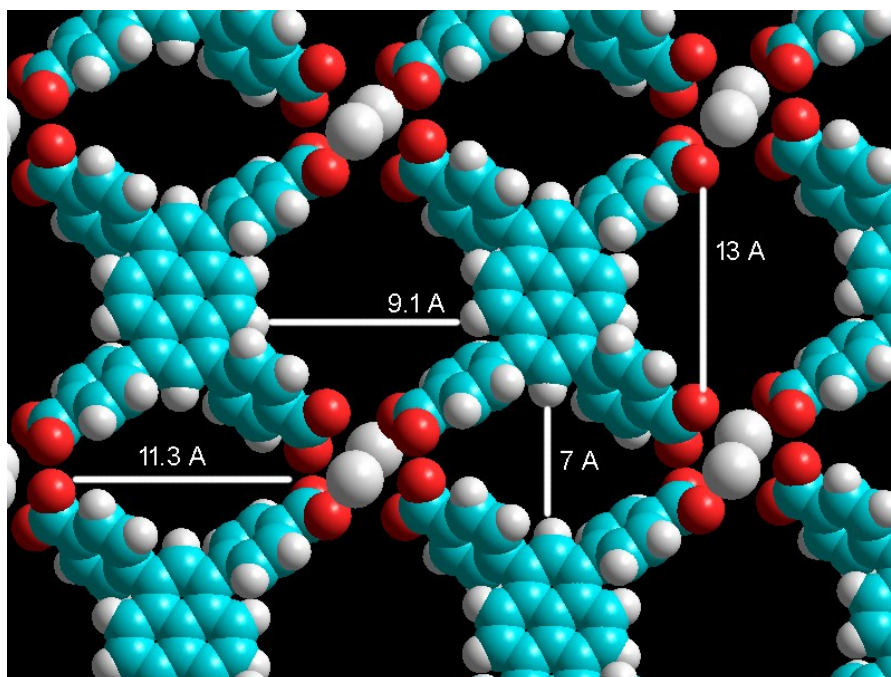


Figure S10. Pore parameters obtained by HyperChem.

The structure was modelled in HyperChem 8.0.8 using molecular mechanics MM+, block-diagonal Newton-Raphson optimization method.

Fluorescence spectra

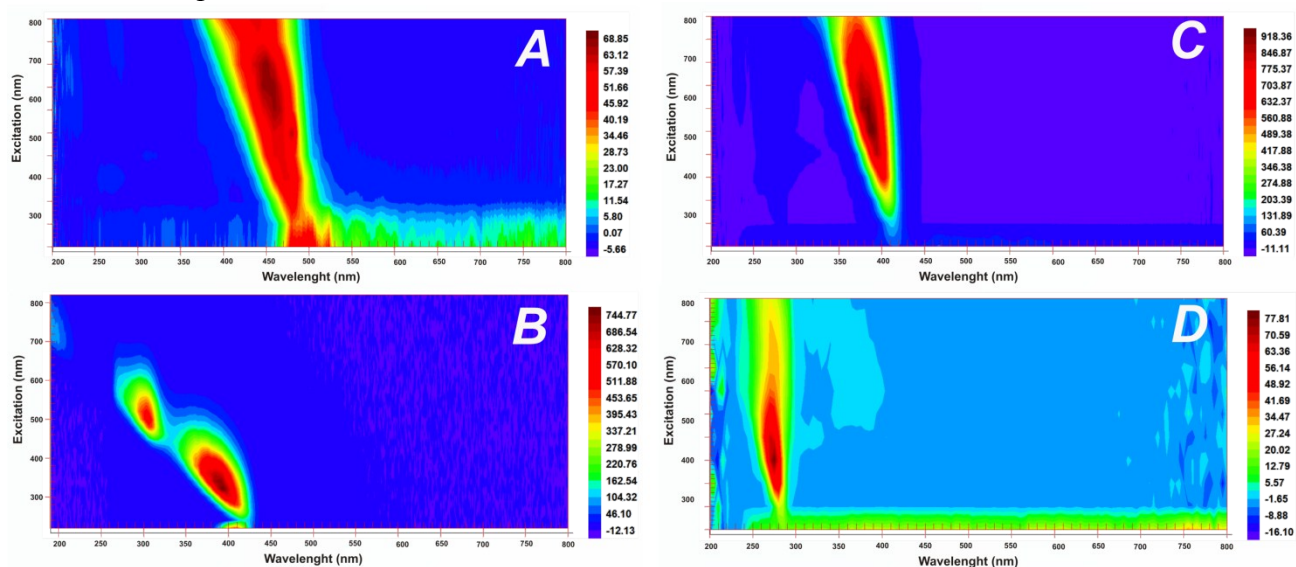


Figure S11. Synchronous 3D fluorescence spectra: A) pure ligand 1,3,6,8-tetrakis(*p*-benzoic acid)pyrene ($c = 0.01$ g/mL), B) $[\text{Zn}_2(\text{TBAPy})]_n$ (**3**) ($c = 0.003$ g/mL), C) L-histidine@ $[\text{Zn}_2(\text{TBAPy})]_n$ ($c = 0.0008$ g/mL), D) L-histidine ($c = 0.2$ g/mL).

2.8 X-Ray structure determination

The data were collected on a Gemini diffractometer (Agilent Technologies) using Mo-K α radiation ($\lambda = 0.71073 \text{ \AA}$) and ω -scan rotation. Data reduction was performed with CrysAlis Pro³ including the program SCALE3 ABSPACK for empirical absorption correction. The structure was solved by direct methods and the refinement was performed with SHELXL⁴. Anisotropic refinement of all zinc and oxygen atoms. Isotropic refinement of the highly disordered carbon backbone (Figures S12). All hydrogen atoms were calculated on idealized positions using the riding model. The formula of the compound may be given as $[\text{Zn}_2(\text{TBAPy})(\text{H}_2\text{O})_2] \cdot 3.5\text{DEF}$ **1**. Basic crystallographic data is summarized in Table S2. Structure figures were generated with DIAMOND-3⁵. CCDC 1409434 **1** contains the supplementary crystallographic data for this paper. The data can be obtained free of charge via www.ccdc.cam.ac.uk/data_request/cif (or from the Cambridge Crystallographic Data Centre, 12 Union Road, Cambridge CB2 1EZ, UK; fax: (+44)1223-336-033; or deposit@ccdc.cam.ac.uk).

All attempts to locate the highly disordered solvent molecules failed. The contribution of the electron density for these highly disordered solvent molecules had been removed with the SQUEEZE routine implemented in PLATON⁶. From the squeeze electron count we suggest to remove the electron density of 7 poorly defined and diffusely oriented DEF (N,N-diethylformamide) molecules ($7 \times 56 = 392$ electrons) from the unit cell. This value corresponds well with the estimated "squeezed" electron density of 405 electrons. A volume of 425 \AA^3 for one DEF molecule (approximately 60 \AA^3 for each non-hydrogen atom) is still acceptable for extremely loosely packed and disordered solvent molecules.

Although TBAPy has only C₂-symmetry in the structure of $[\text{Zn}_2(\text{TBAPy})(\text{H}_2\text{O})_2] \cdot 3.5\text{DEF}$ **1** this linker is located disordered on a $\bar{4}$ -centre (Figure S14). This seems to be a result of the loosely packed layer structure and the highly symmetric coordination mode of the TBAPy ligand itself. The carbon atoms of the carboxylic unit in **1** are separated by 11.89(2) and 12.29(2) \AA (12.078(4) and 12.049(5) \AA for a comparable Zn-MOF²³) indicating a nearly square planar coordination geometry.

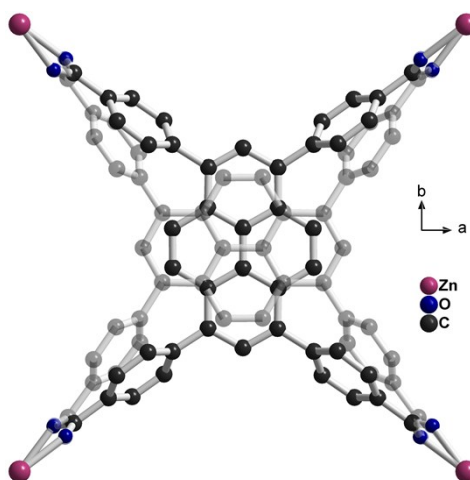


Figure S12. Visualization of ligand disorder: Symmetry operators (x,y,z) $(-x,-y,z)$ for main molecule and $(y,-x,-z)$ $(-y,x,-z)$ for the disordered molecule (transparent)

Table S2 : Crystallographic data of (1)

| | | |
|-----------------------------------|---|---------------------|
| Empirical formula | $C_{61.50}H_{64.50}N_{3.50}O_{13.50}Zn_2$ | |
| Formula weight | 1199.40 | |
| Temperature | 130(2) K | |
| Wavelength | 71.073 pm | |
| Crystal system | Tetragonal | |
| Space group | $\bar{I}4$ | |
| Unit cell dimensions | a = 1569.25(3) pm | $\alpha = 90^\circ$ |
| | b = 1569.25(3) pm | $\beta = 90^\circ$ |
| | c = 1913.79(9) pm | $\gamma = 90^\circ$ |
| Volume | 4.7128(3) nm ³ | |
| Z | 2 | |
| Density (calculated) | 0.845 Mg/m ³ | |
| Absorption coefficient | 0.551 mm ⁻¹ | |
| F(000) | 1252 | |
| Crystal size | 0.2 x 0.15 x 0.1 mm ³ | |
| Theta range for data collection | 3.09 to 25.03° | |
| Index ranges | -18 ≤ h ≤ 18, -18 ≤ k ≤ 18, -22 ≤ l ≤ 22 | |
| Reflections collected | 16639 | |
| Independent reflections | 4162 [R(int) = 0.0627] | |
| Completeness to theta = 25.03° | 98.0 % | |
| Absorption correction | Semi-empirical from equivalents | |
| Max. and min. transmission | 1 and 0.86956 | |
| Refinement method | Full-matrix least-squares on F ² | |
| Data / restraints / parameters | 4162 / 128 / 122 | |
| Goodness-of-fit on F ² | 1.016 | |
| Final R indices [I > 2σ(I)] | R1 = 0.0592, wR2 = 0.1447 | |
| R indices (all data) | R1 = 0.0859, wR2 = 0.1603 | |
| Racemic twin | | |
| Twin domain ratio | 0.51(5) : 0.49(5) | |
| Largest diff. peak and hole | 0.568 and -0.227 e·Å ⁻³ | |

References:

1. Perla B. Balbuena, Keith E. Gubbins, *Langmuir*, **1993**, 9 (7), 1801–1814
2. M.M. Dubinin, in *Progress in Surface and Membrane Science*, edited by D.A. Cadenhead, J.E. Danielli, and M.D. Rosenberg (Academic Press, New York, **1975**), **9**.
3. CrysAlis Pro: Data collection and data reduction software package, Agilent Technologies
4. SHELXL: G. M. Sheldrick, *Acta Cryst. C71* (2015) 3 – 8
5. DIAMOND 3: K. Brandenburg, Crystal Impact GbR, Bonn, Germany
6. PLATON SQUEEZE: A. L. Spek, *Acta Cryst. C71* (2015) 9 – 18